$34 \, p$

SECOND SEMI-ANNUAL PROGRESS REPORT

NASA GRANT NAG8-950

CONVECTIVE FLOW EFFECTS ON PROTEIN CRYSTAL GROWTH

Period of Performance
8/1/93 through 1/31/94

Principal Investigator
FRANZ ROSENBERGER

Co-Investigator
LISA A. MONACO

Center for Microgravity and Materials Research
University of Alabama in Huntsville
Huntsville, Alabama 35899

Summary of Work Performed and Results Obtained

The long-term stability of the interferometric setup for the monitoring of protein morphologies has been improved. Growth or dissolution of a crystal on a 100 Å scale can now be clearly distinguished from dimensional changes occuring within the optical path of the interferometer. This capability of simultaneously monitoring the local interfacial displacement at several widely-spaced positions on the crystal surface with high local depth resolution, has already yielded novel results. We found with lysozyme that (a) the normal growth rate is oscillatory, and (b) the mean growth step density is greater at the periphery of a facet than in its center.

The repartitioning of Na^+ and Cl^- ions between lysozyme solutions and crystals was studied for a wide range of crystallization conditions. A nucleation-growth-repartitioning model was developed, to interpret the large body of data in a unified way. The results strongly suggests that (a) the ion to lysozyme ratio in the crystal depends mostly on kinetic rather than crystallographic parameters, and (b) lysozyme crystals possess a salt-rich core with a diameter on the order of 10 μm.

The computational model for diffusive-convective transport in protein crystallization (see the First Report) has been applied to a realistic growth cell geometry, taking into account the findings of the above repartitioning studies. These results show that some elements of a moving boundary problem must be incorporated into the model in order to obtain a more realistic description.

Our experimental setup for light scattering investigations of aggregation and nucleation in protein solutions has been extensively tested. Scattering intensity measurements with a true Rayleigh scatterer produced systematically increased forward scattering, indicating problems with glare. These have been resolved. Preliminary measurements with supersaturated lysozyme solutions revealed that the scatterers grow with time. Work has begun on a computer program for the unified evaluation of simultaneously obtained, multi-angle static and dynamic light scattering data.

Table of Contents

1. Introduction

Our main research objectives under this grant are:

1. To investigate the effect(s) of defined convective transport and supersaturation conditions on the growth kinetics and morphology of selected proteins.
2. To establish a correlation between the growth conditions, crystallographic quality and x-ray diffraction resolution for some of these proteins.

As outlined in the original proposal, these objectives are to be pursued through work on the following tasks:

1. Refinement of our earlier morphology and kinetics studies without forced flow. In particular, this will be a continuation of our investigations of lysozyme crystal growth.
2. Morphology and kinetics studies under forced flow.
3. Determination of the repartitioning of the precipitant between solution and crystal.
4. Numerical modelling of diffusive-convective transport during protein crystallization..
5. Preparation, purification and compositional analysis of proteins.
6. Measurements of protein/precipitant diffusivities.
7. Measurements of the kinematic viscosity of supersaturated protein solutions.
8. Lights scattering studies of aggregation and nucleation in protein solutions.
9. X-ray diffraction studies of crystallographic quality.

2. Work Performed

During the report period, work was performed on tasks 1- 4, 8 and 9. Details are given in the following sections. Work on task 7 has been concluded; see the First Semi-Annual Progress Report.

2.1. Refinement of Morphology and Kinetics Studies Without Forced Flow

The aim of this work is :

* to provide a basis for comparison with corresponding investigations to be done in the presence of forced flow, and
* to obtain deeper insight into the influences of impurities, step patterns and defects on the growth process.

After the redesign of the microscopic interferometry system described in the First Semi-Annual Progress Report, we have encountered various experimental difficulties. These concerned the geometry and construction of the growth cell, as well as the long-term stability of the interferometric setup and ensuing uncertainties in data interpretation.

The growth or crystallization cell used on the microscope consists essentially of 2 thin microscope cover slips that are spaced by a glass ring. In order to minimize interference fringe formation by the cell, the top and bottom faces of the glass ring and, thus, the cover slips are not parallel. This wedge shape of the cell, however, frequently causes the solution bridge between the cover slips to move from the center of the cell to its narrowest part, where it contacts the sealer between ring and slips. Since we have some experimental evidence that prolonged exposure to such sealers as silicon grease contaminates the solution, we are currently working an a cell design in which the cover slips are either directly fused to the ring or sealed to it with a sealer that was found by others to be DNA compatible.

In the interferometer setup we found that the long-term stability of the solid state laser is inadequate for the high spatial resolution measurements planned. The intensity of the laser jumped several times per day by some ten percent. Since, at that point, intensities at select locations of the interferometric image were recorded from individual pixels only, such jumps severely limited the depth resolution obtainable from intensity time traces. Hence, we have replaced the solid state laser by a highly stable helium-neon laser, and are recording intensities at a location in triplets of pixels which are advantageously spaced across an interference fringe. Correlation of the three intensities of a triplet allow for a clear distinction between intensity changes that are caused by the light source or by dimensional changes within the interferometer

light path. Dimensional changes may be due to actual growth or dissolution of the crystal or dimensional changes of the microscope/interferometer occurring even at the temperature stability of 0.1 °C imposed on the system. To not misconstrue the latter as crystal morphology changes, we have implemented a reference. This reference consists of a triplet intensity trace obtained from a mirror which is positioned on top of the growth cell. After data collection, the up- or down-displacements indicated by the reference trace can be subtracted from the displacements deduced from the crystal surface signal traces. In this way we can detect subtle changes in growth morphologies such as step patterns, growth fronts., etc.

Figure 1 is a sample interferogram obtained from a recent growth experiment with lysozyme. In this experiment, we monitored 5 pixel-triplets positioned on the crystal surface and a reference triplet for several days at various temperatures/supersaturations. A sample of a reference and signal trace obtained during growth at 12°C is shown in Fig. 2a and 2b, respectively. The large spikes in the beginning of both traces are due to known electronic disturbances. The smaller spikes are due to instabilities in data acquisition circuitry and mechanical instabilities in the interferometer.

To eliminate these high frequency disturbances, the traces were digitally filtered through a low-pass Fourier filter. The effects of finite sampling time, typically resulting in significant differences between filtered and original trace at the beginning and end of each sampling period (Gibbs phenomenon), were avoided by applying a Hamming window. Since the filtered traces are the base for calculations of the local face displacement and growth rate, we carefully tested the consequences of the filtering routine. Model traces were generated, corresponding to displacement of the crystal face with constant and with oscillating growth rate. In addition, we superimposed rapid oscillatory and random perturbations on the model signal. We found that the above filtering procedure fully recovers steady and oscillatory displacement inputs. Figure 2c shows the signal trace of Fig. 2b after filtering.

Figure 2d presents the facial displacement at the triplet location obtained on a micron scale from the filtered trace (Fig. 2c) through a continuous phase routine. The displacement of the growth cell of about 600 Å over the whole 120 minutes interval, deduced from the reference trace, was ignored for the calculation of Fig. 2d. The high resolution of the data contained in this displacement trace are illustrated by the corresponding normal growth rate trace depicted in Fig. 2e. Note that the normal growth rate at that location undergoes astonishingly periodic modulation. Such fine-scale modulations cannot be resolved with traditional interferometry in which displacement is measured in terms of the passage of whole fringes, i.e. in steps of order 2,500 Å. In addition, we can obtain the local slope (corresponding to a *mean* growth step

density) by dividing the difference in displacement at two points of a triplet by the distance between them; see Fig. 2f. Finally, as depicted in Fig. 2g, we can calculate the local tangential velocity as the ratio R/p.

The ability to simultaneously monitor the local interfacial displacement at several widely-spaced positions on the crystal surface with high local resolution (within triplets) yields a wealth of information on the evolution of the morphology and its kinetics. For instance, Fig. 3a shows that the local normal growth rate R, at the center and periphery of a crystal facet are about the same over a wide range in supersaturation $\sigma = (C/C_{sat}) - 1$. This confirms that growth on this facet is morphologically stable, i.e. that non-uniformities in the nutrient supply (and, possibly, impurity) field are compensated by non-uniformities in interfacial kinetics. In earlier observations with inorganic crystals as well as lysozyme, the growth step density typically increased with distance from the periphery toward the center of a facet. However, Fig. 3b shows (as is also apparent from the fringe spacings in Fig. 1) that the slope p at the periphery of the crystal and, thus the mean step density is *greater* than in its center. Under these conditions, the observed morphological stability, i.e., the macroscopic shape retention during growth, requires that the tangential velocity in the center of the crystal is higher than at the periphery. This is confirmed by Fig. 3c.

2.2. Morphology and Kinetics Studies With Forced Flow

Parallel to the above efforts, we began to design the flow-through crystallization cell needed for the studies with forced flow. A peristaltic pump has been ordered that can deliver flow rates between 0.003 and 6.7 ml/min. Assuming a 2×2 mm^2 cross-section of the cell, this range corresponds to average flow velocities between 0.012 and 28 mm/sec.

2.3. Repartitioning of Precipitant

Our interest in the repartitioning of the precipitant components between the solution and the growing crystal stems from macroscopic and microscopic considerations. Macroscopically, the repartitioning of precipitant ions could lead to a nonuniform concentration distribution at the growing interface. This, in turn, could induce local changes in the protein solubility and supersaturation, and, hence, should be included in comprehensive model calculations of protein crystal growth; see Section 2.4. Microscopically, we want to shed some light upon the interactions between protein molecules and precipitant ions in the mother solution, in the crystals and the course of crystallization. Nonuniform precipitant capture by the crystal due to variations in crystallization conditions could lead to strain and, consequently reduce the crystallographic perfection.

2.3.1. Findings and discussion

Crystallization experiments were carried out at 4 °C in test tubes containing 10 ml of solution with 2.5 % (w/v) NaCl at pH = 4.5. To clarify the influence of the crystal growth rate on precipitant repartitioning, we used lysozyme concentrations between 8 and 50 mg/ml and corresponding supersaturations $\sigma = (C/C_{sat}) - 1$ between 1.8 and 16. Thus, depending on lysozyme concentration, the ratio of ions to lysozyme molecules in the solution ranged from 780 to 120. The supernatant was separated from the crystals by filtration through 0.22 μm pore size filters. Most crystals remained attached to the test tube walls, the remainder was retained by the filter. To prevent that a solution or adsorption layer adhering to the surface of the crystals biases our measurements, we rinsed the crystals on the walls and on the filter with 1 ml deionized water at 4 °C. This caused slight etching, as revealed by microscopic observation. The rinsing water was added to the supernatant. The filter was then transferred into the test tube and the crystals were dissolved in 10 ml deionized water.

The lysozyme and precipitant ion concentrations were determined in the initial solution, the supernatant and in the dissolved crystals. The lysozyme concentrations were measured by UV spectrophotometry. The Na^+ concentrations were determined with an atomic absorption spectrophotometer, which was zeroed and calibrated, respectively, with dH_2O and 1 ppm Na^+ standard. The initial and supernatant solutions were diluted 1/10,000, while those containing dissolved crystals were diluted 20-200 times depending on protein concentration. The standard was reread after each series of Na^+ determinations of a sample. The Cl^- concentrations were determined by ion selective potentiometry after separation of the lysozyme from the sample by ultrafiltration. Prior to each series of measurements, a new standard curve was obtained for the Cl^- probe. Variations in this curve remained below 5%. A 0.1M Cl^- standard was read before and after each sample reading to check probe stability. It should be emphasized that the amounts of lysozyme, Na^+ and Cl^- in the crystals were *directly* determined, rather than as differences between the concentrations in the initial and supernatant solution. In order to check the preservation of component masses, we have carefully measured the solution volumes used in all steps of the procedures. The sum of the quantities of lysozyme, Na^+ and Cl^- was retained within 5% in all runs. Since this simply represents the sum of the uncertainties involved in the three-step analyses, this mass balance gives us additional confidence in our procedures.

To estimate a possible systematic error in our determination of the protein and the precipitant ions, especially when small crystal quantitites were analyzed, we performed two control experiments. One test tube containing 10 ml of deionized water and another one with 11 mg/ml lysozyme solution with buffer and precipitant, were kept at 4 °C for only ~15 min, so that

no crystals formed in the second tube. Then both tubes' contents were analyzed for protein and Cl⁻ following the full procedure described above, including filtration and rinsing. The results obtained for the processed pure water sample indicated no salt or protein pickup in our procedure. In the second control experiment, we found 0.2 mg of lysozyme and 0.7 μmol of Cl⁻ that probably adhered to the tube walls or the filter even after rinsing. Hence, even with the smallest amount of crystals analyzed in our experiments (3.4 mg or 0.25 μmol) the crystallized lysozyme amount would only be too high by 6%, and the number of ions per lysozyme molecule by three.

The experimental results for Na⁺ and Cl⁻ ions were expressed as molecular number ratios $n = N_{ion}/N_{lysozyme}$ found in the crystal, the supernatant and the initial solution. We also calculated effective segregation coefficients $k = (N_{ion}/N_{lysozyme})^{cryst}/(N_{ion}/N_{lysozyme})^{soln} = n^{crys}/n^{soln}$. As in section 2.1, supersaturation was defined as $\sigma = (C/C_{sat}) - 1$, where $C_{sat} = 2.8$ mg/ml is the lysozyme solubility at our working temperature as determined in a batch experiment.

In the first series of experiments, the crystals were separated from the supernatant after between 3 and 10 % of the protein had crystallized. The measured dependence of n on supersaturation is shown in Fig. 4. One can see that:

(a) At low supersaturations $n^{crys} \approx 100$. This is much higher then one would expect either from the charge of the lysozyme molecule (≈ 12 at our pH = 4.5), the number of polar groups on the surface of the molecule, or from results of calorimetric investigations of Cl⁻ /lysozyme interactions.

(b) At high supersaturations n^{crys} is much lower than at low ones. Intuitively, one would expect the opposite. Higher supersaturations lead to higher crystal growth rates, which, in inorganic systems, are usually associated with higher defect concentrations. Thus, precipitant ions could be more readily accommodated in the lattice.

(c) The n^{crys} for Cl⁻ is always somewhat lower than for Na⁺ ions. This difference, which could be associated with the ultrafiltration, requires further investigation.

(e) Rinsing did not significantly affect the Cl⁻ and Na⁺ concentrations. Hence, we conclude that the higher values are not due to a surface effect.

(f) The reproducibility in the experimental data is somewhat lower than expected from the standard deviations of the analytical methods employed. This could be due to a possible dependence of n on the fraction of lysozyme crystallized, which, as mentioned above, varied from 3-10%.

To explore whether n^{crys} depends on crystallized fraction, we measured the captured ion quantities versus crystallization time. Six test tubes were filled with solution of the same initial C_{lys}. From this set, tubes were removed at increasing times, and their contents analyzed. Such measurement series were carried out with three initial supersaturations, $\sigma_0 = 3.2$, 5.4 and 13.1. The n^{crys}-values obtained at $\sigma_0 = 5.4$ and 13.1, i.e., for initial $C_{lys} = 18$ and 38 mg/ml, respectively, are shown in Fig. 5. At the shortest crystallization times, n^{crys} roughly agrees with the values of Fig. 4 at the same supersaturation. Then it sharply drops, approaching ≈ 10 times lower values at long crystallization times. This strong time dependence of n is likely the reason for the limited reproducibility of the data in Fig. 4.

The decrease of n with crystallization time could be due to the diffusion of captured ions back into solution. To check this hypothesis, we carried out experiments with ten tubes containing the same initial $C_{lys} = 18$ mg/ml, i.e., $\sigma_0 = 5.4$. Tubes were removed from the refrigerator in pairs at increasing times. Each time, the crystal in one of the tubes were immediately analyzed. However, the second tube was placed for six days into an incubator at saturation temperature, and then the crystals were analyzed. Figure 5 shows that there is essentially no difference between n^{crys}'s obtained from the two sets of tubes. Hence, back-diffusion of captured precipitant ions to the solution cannot be the reason for the observed decreasing concentrations with increasing crystallization time.

Another possible reason for the decreasing n^{crys} could be protein aggregate formation. Sedimentation, light scattering and dialysis kinetics studies have shown that in crystallizing lysozyme solutions the molecules form dimers, tetramers, octomers, etc. It is feasible that larger aggregates will associate with fewer ions/molecule since some of the possible binding sites take part in protein-protein contacts. Hence, higher concentrations of larger aggregates that might form with time could lead to larger ensembles entering the crystal and, thus, to a decrease in n^{crys} either with time or increasing supersaturation. Yet, evidence to be presented below, suggest against this possible mechanism.

In order to explore whether the decreasing supersaturation is responsible for the time dependence of ion incorporation, we have plotted in Fig. 6 all data obtained without incubation, as a function of the final supersaturation at the separation of the crystals, σ_f. Note that for specific data points, the crystals grew at supersaturations between the specific σ_f and the σ_0 of the series. Since the three data groups do not coincide in the overlapping regions of supersaturation, this representation clearly demonstrates that the decrease in ion incorporation is not simply following the decrease in supersaturation. However, a plot of these data in terms of $k(\sigma_f)$ in Fig. 7 reveals some similarity of the data. One sees that the values of the initial and final

segregation coefficients, rather independent of supersaturation, are $k_0 = 0.1$ and $k_f = 0.003$, respectively. Hence, it appears that the amounts of precipitant ions captured in the lysozyme crystals is largely determined by the ratio of ions to protein molecules in the solution, rather than by crystallographic factors only.

To provide additional support for the above conclusion, we performed experiments with doubled NaCl concentration (5 % w/v) and, thus doubled ratio of ions to lysozyme molecules in the solution. The experiments were carried out at 18 °C, pH = 4.5 as before, and lysozyme concentrations of 14.9, 19.9 and 37.1 mg/ml. Thus, as shown in Table 1, the initial supersaturations were $\approx$ 1.5 times higher than in the series with 2.5 % NaCl solutions at 4 °C. If the ratio in the solution is the driving force for ion incorporation in the crystals, we would expect higher capture in the experiments with 5 % salt. On the contrary, if supersaturation is the main factor, we would expect, in analogy to Fig. 4, lower incorporation. Table 1 shows that the k-values obtained from the solutions with different salt concentrations are essentially the same, while the n^{crys}-values increased proportionally to the salt concentration.

Another similarity between the three data sets in Fig. 7 is suggested by the increasing curvature of $k(\sigma_f)$ with decreasing σ_0. Hence, we have replotted the data in Fig. 8 in terms of the normalized supersaturation σ_f/σ_0. This normalization reduces the three data sets to one. Thus, the time (or σ_f) dependence of ion incorporation is apparently also governed by σ_0. On the other hand, σ_0 is an essential parameter in the nucleation and growth kinetics underlying these repartitioning processes. Therefore, in the following, we will attempt to correlate ion incorporation to the nucleation and growth kinetics underlying the above three series of experiments.

In Fig. 9 we present the time dependence of the crystallized fractions of protein, that were calculated from the measured lysozyme concentrations in the initial solutions and supernatants. In comparing these dependencies to the corresponding $n^{crys}(t)$ in Fig. 5, one notes that higher salt incorporation occurs in the same time span as the steep increase in the fraction crystallized. As we will quantitatively show below, this exponential increase denotes the regime in which nucleation dominates over the growth of existing crystallites. Hence, we assume that newly nucleated, small crystals capture a larger amount of precipitant per lysozyme molecule than the ensuing growth to larger sizes. Thus, ion rich cores are surrounded by crystalline shells that are leaner in salt.

To decide between coring, and aggregation in the solution, we performed a new set of experiments with seeded and unseeded solutions with C_{lys} = 12 mg/ml. As seeds we used

crystals formed in a 50 mg/ml solution, which, according to the trend represented by Figs. 4 and 6, possess low ion contents even in the "core". In four seeded tubes, up to 70 % of the protein crystallized in 2 days. In four unseeded tubes, crystals appeared only after 3 days. The results obtained for various crystallized fractions are shown in Fig. 10. In the seeded solutions n^{crys} stayed essentially constant. (Note that some minimal growth onto the seeds is required, hence the lack of data for seeded runs at σ_f/σ_0-values close to unity). The unseeded runs show again the initial high incorporation, dropping with time to the same value as in the seeded runs. For the aggregation mechanism we would expect lower incorporation in the unseeded experiments since there crystals grew from older solutions. Hence, the results do not support this mechanism, but rather the concept of coring. With the introduction of low-salt seeds, formation of the salt-rich core, typical for the low supersaturation used, was apparently suppressed. This led to the rather constant n^{crys} versus fraction crystallized.

In the following we will shows that all above data are quantitatively compatible with results obtained from a model which combines the nucleation and crystal growth aspects of the experiments with the assumed formation of salt-rich cores in the crystals.

2.3.2. Nucleation-growth and salt incorporation model

We assume that the nucleation of crystals can be described by classical nucleation theory. The nucleation flux J in $[cm^{-3}s^{-1}]$ is

$$J = 4\pi R_c^2 C^2 \kappa Z a \exp\left(-\frac{F_c}{kT}\right). \tag{1}$$

Here R_c is the radius of the critical 3D nucleus

$$R_c = \frac{2\Omega\alpha}{\Delta\mu} \cong \frac{2\Omega\alpha}{kT\ln(C/C_{sat})} , \tag{2}$$

where Ω is the volume one molecule occupies in the crystal, α is the free surface energy of a crystal in contact with the supersaturated solution; C is the concentration, κ is an attachment parameter, a is the dimension of a molecule, Z is the Zeldovich factor

$$Z = \left(\frac{F_c}{3\pi kTN_c^2}\right)^{\frac{1}{2}} , \tag{3}$$

where s is the thermodynamic supersaturation $s = \Delta\mu/kT \cong \ln(C/C_{sat})$ and F_c is the free energy barrier for nucleus formation,

$$F_c = \frac{16\pi\Omega^2\alpha^3}{3\pi(kTs)^2} . \tag{4}$$

Combining (1)-(4), and denoting all parameters independent of supersaturation and concentration as A and B, we get for J

$$J = A \, C^2 \exp(-B/s^2) \ . \tag{5}$$

Based on our previous growth rate measurements, we assumed two types of quantitative dependencies of the crystal growth rate R on supersaturation:

(a) R is a linear function of supersaturation $\sigma = (C/C_{sat}) - 1$, except for a dead zone for $\sigma < 0.7$, where it vanishes:

$$R = 10^{-8} (\sigma - 0.7) \, \text{cm/s} \ . \tag{6}$$

(b) R is a parabolic function of the thermodynamic supersaturation for $s \leq 2$, and linear with s for higher supersaturations:

$$R = 0.26 - 1.55s + 1.73s^2, \quad s \leq 2 \ , \tag{7a}$$

$$R = 1.6 + 2.2s \ , \qquad\qquad s > 2 \ . \tag{7b}$$

The above dependencies reflect the functional form found for higher temperatures [Vekilov et al., 1993; Monaco and Rosenberger, 1993]; the numerical values, however, were adjusted to give realistic results for the 4 °C used in our experiments. For calculations of the crystallized fraction, we have assumed that growth on each nucleus occurs in the form of a cube, the linear dimensions of which are governed by the normal growth rates of eq. (6) or (7). It should be noted that the above growth morphology studies with lysozyme have shown that the growth kinetics is much slower than transport kinetics. Hence, this system well fulfills the uniform concentration assumption underlying all above relations.

This model was evaluated for the lysozyme solubility and initial concentrations used in the experiments. For Ω we took the value 2.7×10^{-20} cm^3 for lysozyme. The experimental crystallization times were divided into 150 steps. Doubling of the number of time steps caused only minor changes in the results. In each step we updated the calculated crystallized fraction and supersaturation within the finite volume of 10 ml. The new supersaturation was then used to calculate the nucleation flux and the crystal growth rate in the next step; etc.

Since reliable values of the parameters (α, ν, E) governing the nucleation of lysozyme are not available, we fitted the theoretical dependence of the crystallized substance on time resulting from eq. (1)-(7) to the experimental data for $C_{lys} = 18$ mg/ml, and thus determined the parameters A and B in eq. (5). Then we calculated the curves for $C_{lys} = 12$ and 38 mg/ml employing the same values of A and B. The model curves obtained with both R(σ) relations are shown in Fig. 9, with dashed and solid lines for the solutions obtained with eqs. (6) and (7),

respectively. One sees that the best fits to the experimental data result from the more realistic quadratic relation, eq. (7). We also calculated the average size of the crystals at different stages of crystallization. The calculated sizes agree well with the observed ones. The good correspondence between the numerical and experimental results supports the applicability of this nucleation and growth model to our system.

In the simulations of the Na^+ and Cl^- ions incorporation we simplified matters by assuming that each lysozyme molecule enters the crystal with the same number of both ions. This number for freshly formed crystals, N_0, was assumed to be larger than the corresponding number for large crystals, N_f, in order to account for the suspected coring. The drop from N_0 to N_f was assumed to follow a specific functional dependency until a crystal reached a specific size $2L_c$. The values of N_0 and N_f were obtained for each initial supersaturation by multiplying the respective n^{soln} by $k_0 = 0.1$ and $k_f = 0.003$. In each simulation step, we updated the quantity of ions and lysozyme in the solution and growing crystal to obtain average numbers n^{crys} and segregation coefficients k.

We used various combinations of L_c-values and functional dependencies of the drop from N_0 to N_f on crystal size. Best agreement with the experimental data in Fig. 8 was achieved with an exponential dependence and L_c's of about 20 μm, which lead to the three almost indistinguishable solid lines in Fig. 8.

The evidence for a salt-rich cores in lysozyme crystals presented above is strong. Such coring could have far-reaching consequences. For instance, coring could introduce considerable strain, which, in turn, could be one reason for limited diffraction resolution. On the other hand, such coring has not been observed before in protein crystals, possibly due to the relative smallness of the cores. Hence, before we embark on further speculations, we must either prove or disprove the above model explanations of the unusual repartitioning results by some independent experimental technique. Best suited for this crucial test would be a technique that directly yields a compositional profile across a (sectioned) crystal, rather than another averaging analytical technique. We are currently evaluating various options.

2.4. Numerical Modelling of Diffusive-Convective Transport

In order to shed some light on the role of convection in protein crystallization, we have developed a time-dependent, two-dimensional model of convective-diffusive transport in the solution coupled with interfacial growth kinetics. This model provides insight into the evolution of the concentration distribution of the various species present in the nutrient solution, growth

rate distribution across facets, and the precipitant distribution in the growing crystal. The interplay between transport and growth morphology dependent kinetics will be included in the future.

The model, numerical approach and preliminary results were presented in detail in the First Semi-Annual Progress Report. Since then, the efficiency of the numerical solution procedure has been considerably improved. As a consequence we have been able to expand the simulation of lysozyme growth experiments from one to five hours in real time. This has revealed that our model does not describe the long-term aspects of the crystallization process too well. We had originally argued that, since the face growth rates of protein crystals are low, a constant crystal size would lead to about the same concentration and growth rate distributions as one would obtain from a much more complex moving boundary description. This is true for the first hour of crystallization time. For longer growth times, however, the gain in crystal size is not small compared to the solution layer width between crystal and upper wall of the growth cell. Thus significant deformations of the concentration fields in the solution occur.

These shortcomings of our model are being remedied by incorporating a pseudo-moving boundary approach. While the shape of the crystal is still not allowed to change, the crystal size and the location of grid lines are periodically updated according to the average growth rate of the crystal facets. It appears from the first test runs with this modified algorithm, that the additional computer time required by this more realistic approach is reasonable.

2.5. Light Scattering Studies

The objective of our light scattering studies is to gain more insight into the aggregation phenomena occuring in supersaturated protein solutions. We want to perform simultaneous dynamic and static light scattering experiments at several scattering angles. Concurrently we are developing a new analysis procedure to combine both static *and* dynamic data into a single analysis of the underlying particle size distribution (PSD).

In our current set-up we can perform measurements at different angles only sequentially which imposes an important restriction on our time-resolution. We therefore wanted to clarify if we can collect multiple-angle data in a time span short compared to typical changes of the PSD in the solution. These experiments should also tell us about the amount of additional information gathered through multi-angle dynamic and static light scattering.

In a typical run we perform measurements of one minute duration each, at fourteen different scattering angles, between 15° and 150°. Such a scan is repeated every 30 minutes. The

correlator is set to collect data at four different sample times (multiple-tau option) covering a range of diffusion constants D approx. between 10^{-6} cm^2/s and 10^{-8} cm^2/s. For diffusing particles, the decay time $\tau_D(q)$ associated with the exponentially decaying autocorrelation function is

$$\tau_D(q) = \frac{1}{Dq^2} \quad , \tag{1}$$

where $q = 4\pi n/\lambda \, \sin(\theta/2)$ is the magnitude of the scattering vector at some scattering angle θ. The shortest sample time at each angle was adjusted to follow that behavior. Data were collected with a supersaturated lysozyme solution at 50mg/ml concentration, pH 4.5 and 2.5% NaCl (by weight). The temperature during the first two scans was kept at 20 °C and was lowered to 15 °C for all scans thereafter. The experiment took 6 hrs after the sample was put into the thermostat.

After subtracting the baseline from the dynamic data, the measurements at various angles can be combined into a single plot if we rescale the time axis by the ratio

$$\frac{\tau_D(\theta)}{\tau_D(90)} = \frac{1/2}{\sin^2(\theta)} \tag{2}$$

to eliminate the inherent q^2-dependence given in eqn.(1). The choice of 90° as reference angle is arbitrary .

Figures 11 and 12 show, respectively, the rescaled intensity autocorrelation functions from the first and the last scan at 15°C of the above experiment. In Fig. 11, data from different angles collapse onto a single curve indicating that we gain no extra information from multiple scattering angles. Figure 12 clearly shows the break-down of this scaling in the later stages of nucleation. We can understand this by recalling the relationship between the field correlation function and the particle size distribution

$$g_1(\tau) = \sum_{i=1}^{\infty} \rho_i \, m_i \, S(q,r_i) \exp[-D_i q^2 \tau] \quad , \tag{3}$$

where ρ_i, m_i and D_i are the weight fraction, molecular weight and diffusion constant of particles with radius r_i, and $S(q,r_i)$ is the static structure factor. In the Debye-Gans approximation for solid spheres we obtain

$$S(q,r) = \left[\frac{3[\sin(qr) - qr \, \text{Cos}(qr)]}{(qr)^3} \right]^2 \quad . \tag{4}$$

As long as the particles are Rayleigh-scatterers (qr << 1 in eqn. (4)), they scatter with a fixed amplitude into all directions within the scattering plane. Under these circumstances $S(q,r_i)$ has no angular dependence. When scatterers grow beyond that limit, intraparticle interference becomes important and large particles scatter predominantely into the forward direction. (Once

the particles become true Mie-scatterers several intensity maxima and minima develop in the scattering plane, modifying this simple picture).

Figure 13 presents the relative intensity data corresponding to the dynamic data of Figs. 11 and 12, respectively. Since the scattering column is cylindrical, the intensity was rescaled to the size of the scattering volume V_s at some reference angle. For our instrument the proper correction is

$$\frac{V_s}{V_{90}} = \frac{1}{\sin \theta} \cdot$$

(5)

Again the scattering volume at 90° is chosen as arbitrary reference point. As indicated above, the intensity for a Rayleigh scatterer is independent of the scattering angle. Even at the earliest stage, however, we see a slight increase (3%) in the forward direction with a jump at 15°, which is probably due to glare from the glass/solution interface. With time, the shallow peak becomes more pronounced and spreads to the larger scattering angles, while the overall intensity keeps increasing as well. Similar behavior was seen in several equivalent experiments and implies the presence of some larger aggregates early on, which are growing in size.

The conclusions from these preliminary runs are the following. Multiple angle dynamic and static data do contain valuable supplementary information. They also suggest a certain experimental protocol. We will start with solutions that are undersaturated at room temperature. Taking several angular scans at this point should identify the presence of any preexisting aggregates introduced through the sample preparation and will establish a background scattering intensity. Then we can reduce the temperature into the supersaturated regime and follow the time development of the aggregation process. Thermodynamically reversible and irreversible changes could be distinguishable by bringing the sample back up to the undersaturated state.

In parallel to the experimental efforts we are working on an algorithm for a combined analysis of our static and dynamic data. We have tested one of the most sophisticated codes for PSD-analysis of dynamic light scattering data, CONTIN, and subjected it to a series of tests with computer generated and experimental data. This provided us with several important insights. First of all, the inversion process is very sensitive to a variety of different experimental and numerical parameters. These include the sample times, background intensity, scattering angle, the choice of particle-size interval for the inversion process, the number of particle sizes within this interval, and, most of all, the noise in the data. This should not be considered a shortcoming of the algorithm, but reflects the ill-posed character of the problem in the presence of noise. However, there are some specific properties of CONTIN which convinced us to pursue a

different analysis scheme: CONTIN is based on the Laplace inversion of the field correlation function. We would like to analyze the intensity correlation function instead, which is less noisy (see First Report for details), but can not be used for Laplace inversion. Furthermore, this algorithm is highly sophisticated and therefore time-consuming to modify and provides no obvious way to incorporate intensity information.

Hence, we are currently adopting an algorithm based on work by Cummins and Staples (Langmuir 3, 1987, p.1109). A Fortran version has been made available to us by Prof. Cheung at the University of Akron, Ohio. It assumes a fixed distribution of particle sizes with the scattering amplitude for each size as fitting parameter. The program performs a nonlinear least-squares fit to the data by adjusting these amplitudes and calculating the resulting shape of the field correlation function. There is no intrinsic reason one couldn't fit the intensity correlation function, instead. Multiple angle data can be incorporated in a straight-foreward fashion. It is also easy to see how to incorporate the static scattering intensity into the analysis: For a given distribution of particle sizes one calculates both the corresponding autocorrelation function and scattering intensity and requires a fit consistent with both sets of data. The porting of the code to our system, the proposed modifications, and testing of the output are part of ongoing work.

During the last half year we have implemented a variety of improvements in our experimental set-up. The mounting of the laser underneath the optical bench was modified to reduce vibrations. These vibrations had caused small changes in beam intensity as the beam position varied on various optical components. Right now our laser power, measured at the input to our sample thermostat, remains stable to within ± 0.5% for several hours. Furthermore, we have purchased a new sample cell holder from Brookhaven Instruments. It features a conical teflon sleeve assuring repeatable, accurate positioning of different sample cells in the same location. The teflon sleeve also protects the cells from scratching during mounting and removal. At the same time, we modified the sample thermostat to accept large diameter scintillation vials, which will reduce the glare-problem at small scattering angles. In addition, an improved alignment procedure was developed for the goniometer set-up. It allows for mechanical and optical alignment of the apparatus in shorter time and with higher accuracy, while circumventing some shortcomings of the manufacturer's suggested procedure. The final alignment is tested with a Rayleigh scatterer (toluene). Down to 30° the scattered intensity is constant within 1%, at 15° it increases by 4% compared to the value at 90°.

3. Presentations, Publications and Other Professional Activities

Presentations

P.G. Vekilov, M. Ataka and T. Katsura, *Growth kinetics of protein crystals investigated by laser Michelson interferometry;* talk at the Conference on Protein Crystal Growth in Microgravity, Panama City, Florida, April 23-26, 1993.

P.G. Vekilov, M. Ataka and T. Katsura, *Interferometric studies of protein crystal growth;* invited talk at the 5-th International Conference on Crystal Growth of Biological Macromolecules, San Diego, California, August 11, 1993

P.G. Vekilov, *Dislocation source activity in growth and dissolution of crystals from solution;* talk at the 7-th Annual Alabama Materials Science Conference, Huntsville, Alabama, September 25, 1993.

L.A. Monaco, F. Rosenberger, *Growth kinetics and morphology of tetragonal lysozyme;* invited talk at the Protein Crystal Growth in Microgravity Conference, Panama City Beach, Florida, April 23-26, 1993.

L.A. Monaco, Hong Lin, A. Nadarajah, F. Rosenberger, *Convective flow effects on protein crystal growth diffraction resolution - A research plan;* The Protein Crystal Growth in Microgravity Conference, Panama City Beach, Florida, April 23-26, 1993.

L.A. Monaco, F. Rosenberger, *Kinetics and morphology of protein crystal growth;* Biology Seminar, Brookhaven National Labs, Long Island, New York, June 4, 1993.

L. Monaco, P. Vekilov, F. Rosenberger, *Kinetics, morphology and segregation in lysozyme crystallization;* invited talk at Fifth International Conference on Crystallization of Biological Macromolecules, San Diego, California, August 8-13, 1993.

L.A. Monaco, P. Vekilov, F. Rosenberger, *Kinetics, morphology, and segregation in lysozyme crystallization;* 7-th Annual Alabama Materials Science Conference, Huntsville, Alabama, September 21, 22, 1993.

Other Related Professional Activities

Franz Rosenberger has organized and chaired a session on Physics of Crystallization at the Fifth International Conference on Crystallization of Biological Macromolecules, August 8-13, 1993 in San Diego, CA. He has also been elected president of the Advisory Board for the Sixth International Conference on Crystallization of Biological Macromolecules, to be held in October 1995 in Kyoto, Japan. Furthermore, Rosenberger has been invited to present a plenary lecture on "Protein Crystallization - What We Should Know, and What We Do Know" at the Eleventh International Conference on Crystal Growth in Arnhem, Holland, in June 1995.

Table 1. Comparison between the incorporation of Na^+ and Cl^- in lysozyme crystals at two different NaCl concentrations and temperatures.

	5 % NaCl / 18 °C			2.5 % NaCl / 4 °C		
C_{lys}	14.9	19.9	37.1	18.0	18.0	38.0
σ	7.3	10.2	19.8	5.4	5.4	13.1
n^{soln}	830	630	340	340	340	164
fraction crystallized	0.16	0.11	0.09	0.16	0.11	0.09
$n^{crys}_{Na^+}$	18.5	26.7	20.4	8	13	10
$n^{crys}_{Cl^-}$	15	22.6	15.1	6	9	7
k_{Na^+}	0.022	0.041	0.060	0.023	0.038	0.061
k_{Cl^-}	0.018	0.036	0.045	0.017	0.026	0.042

100 μm
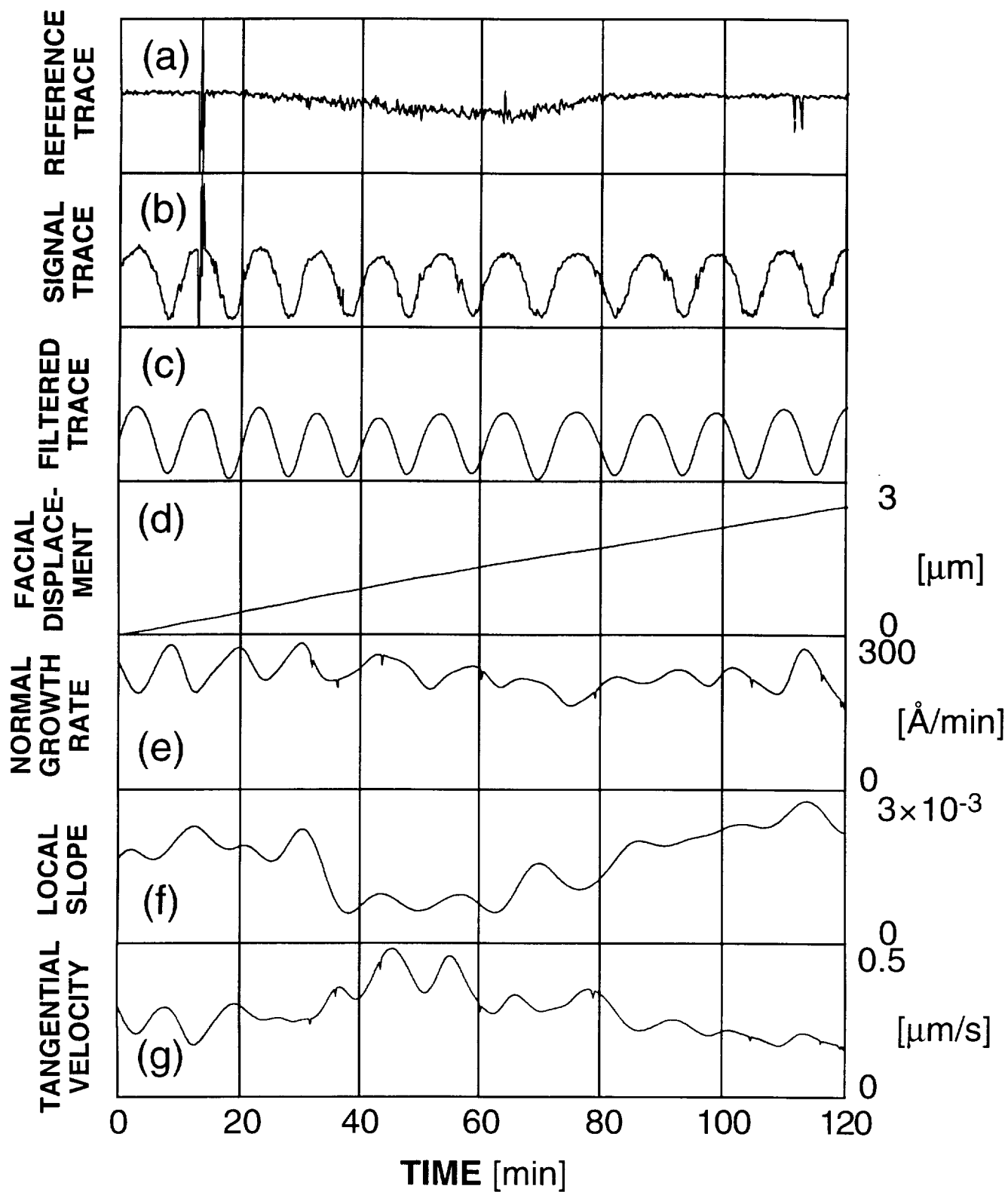
FIG. 1

FIG. 2
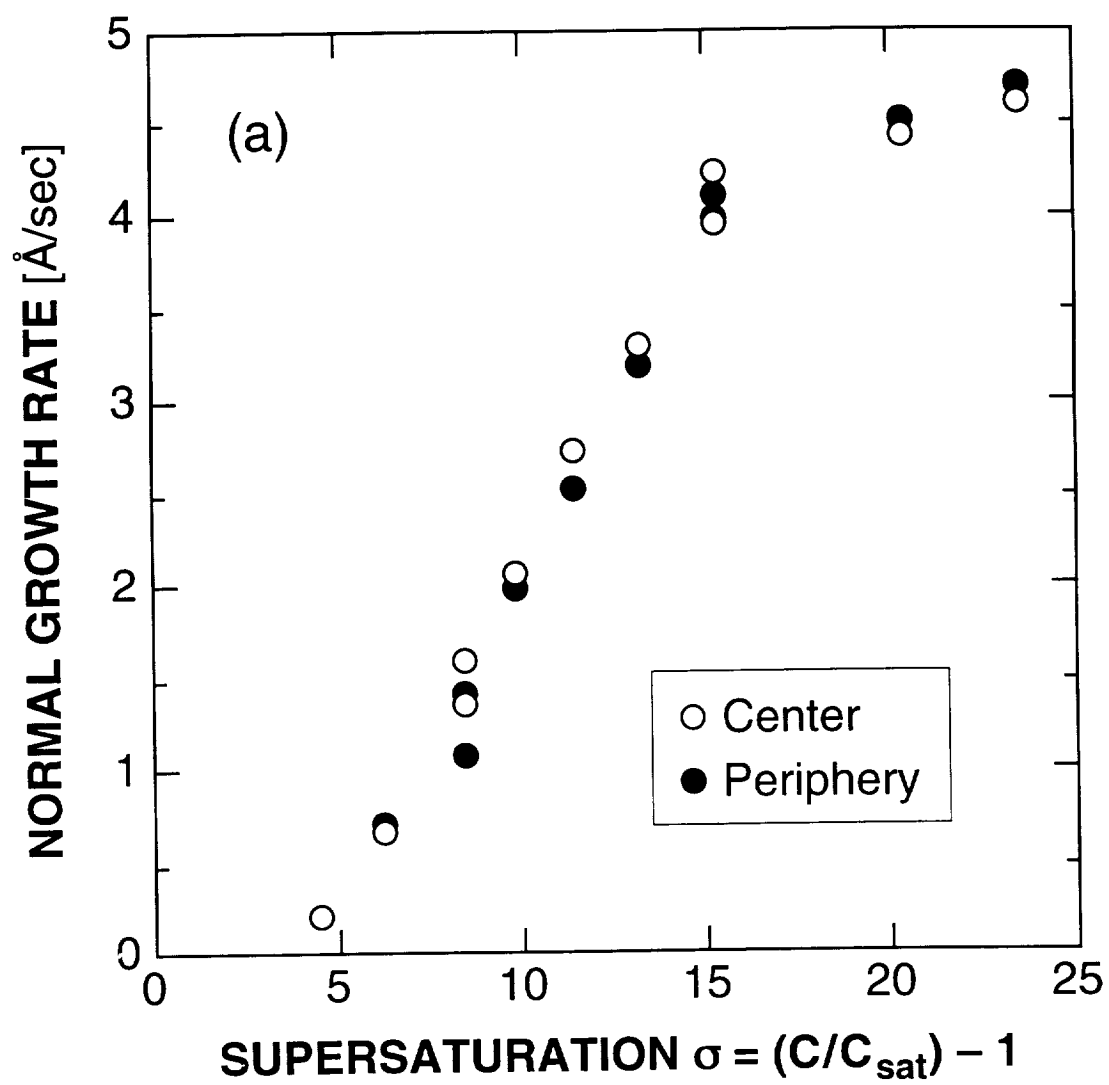
FIG. 3a
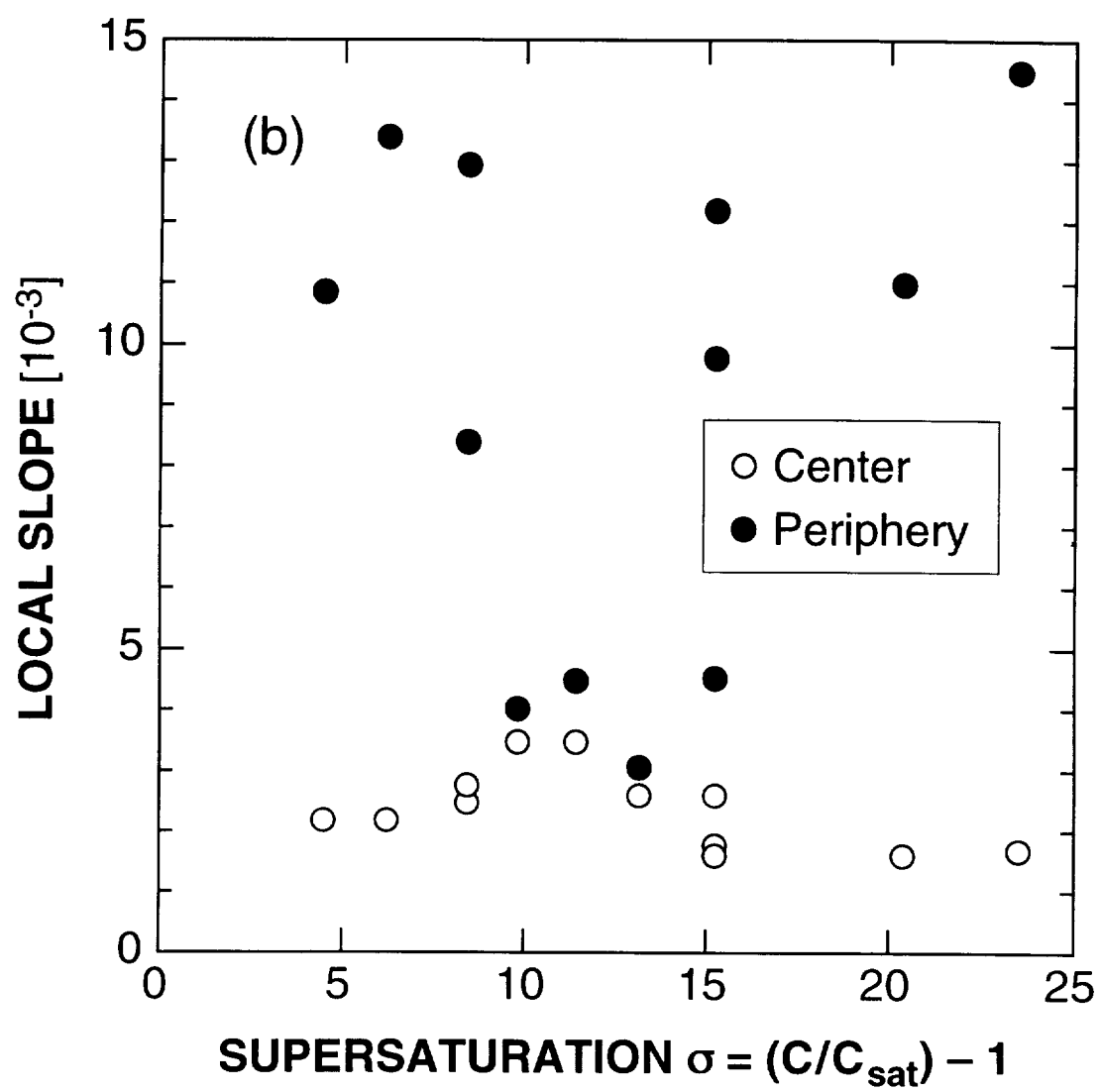
FIG. 3b
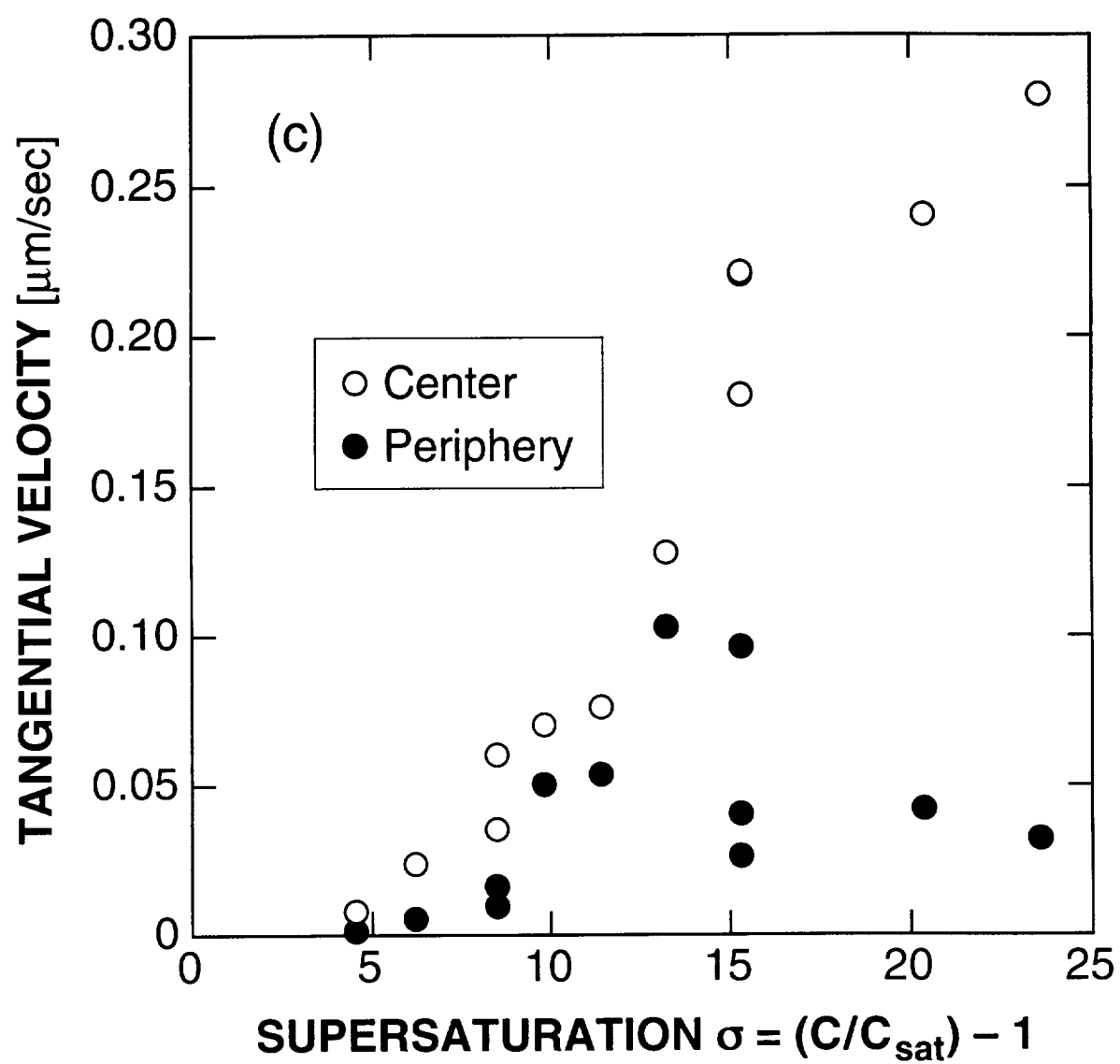
FIG. 3c
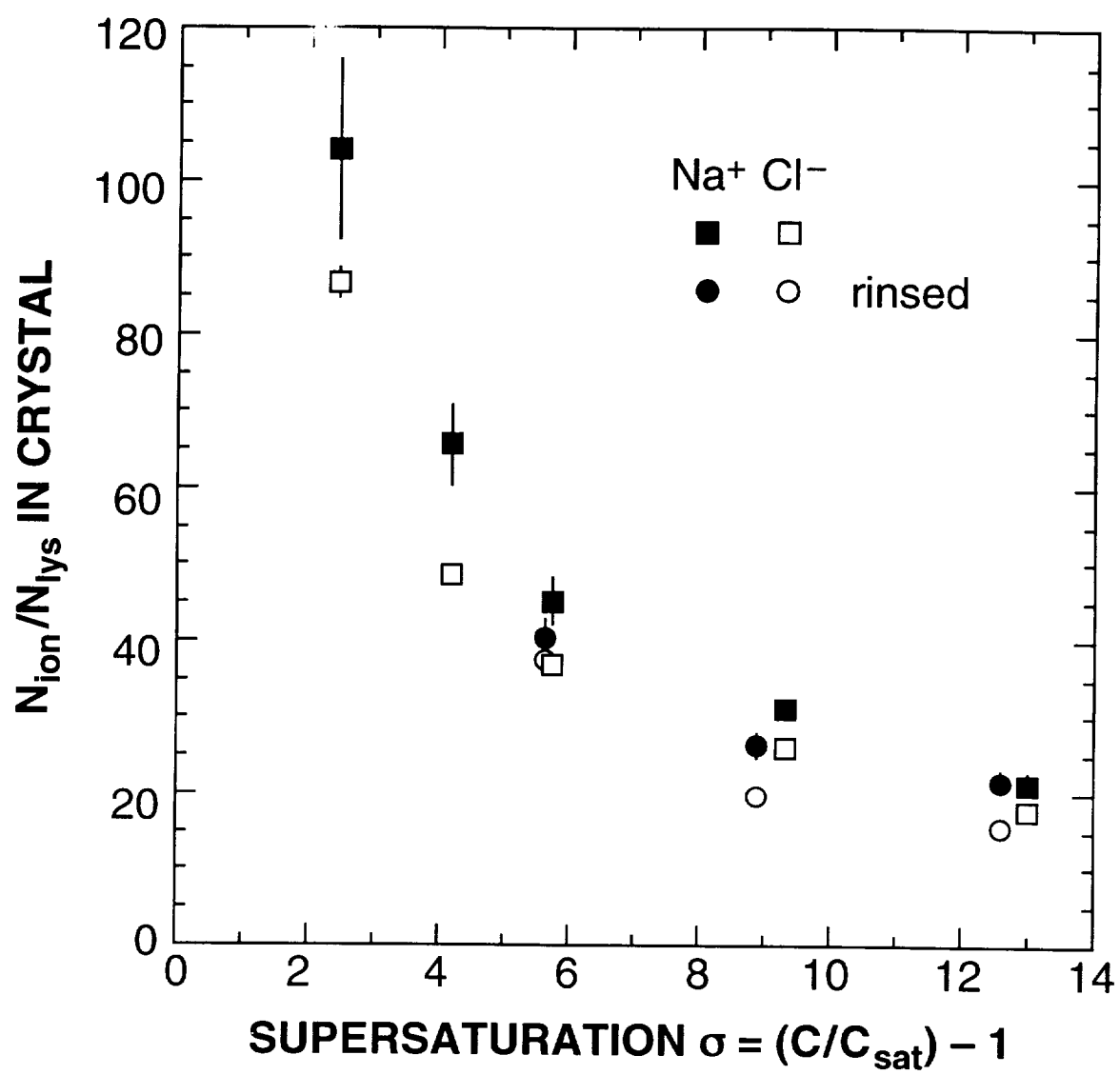
FIG. 4
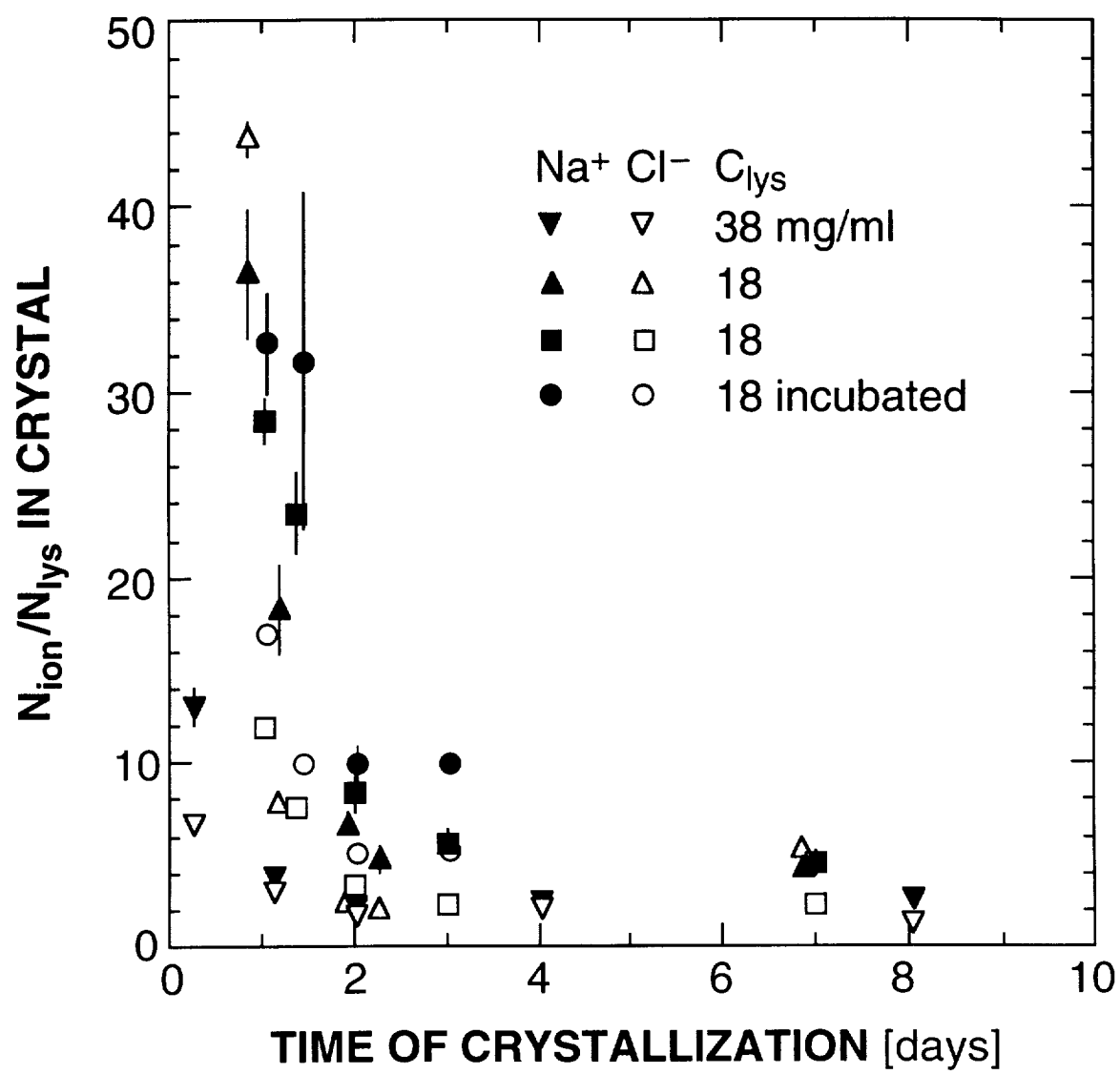
FIG. 5
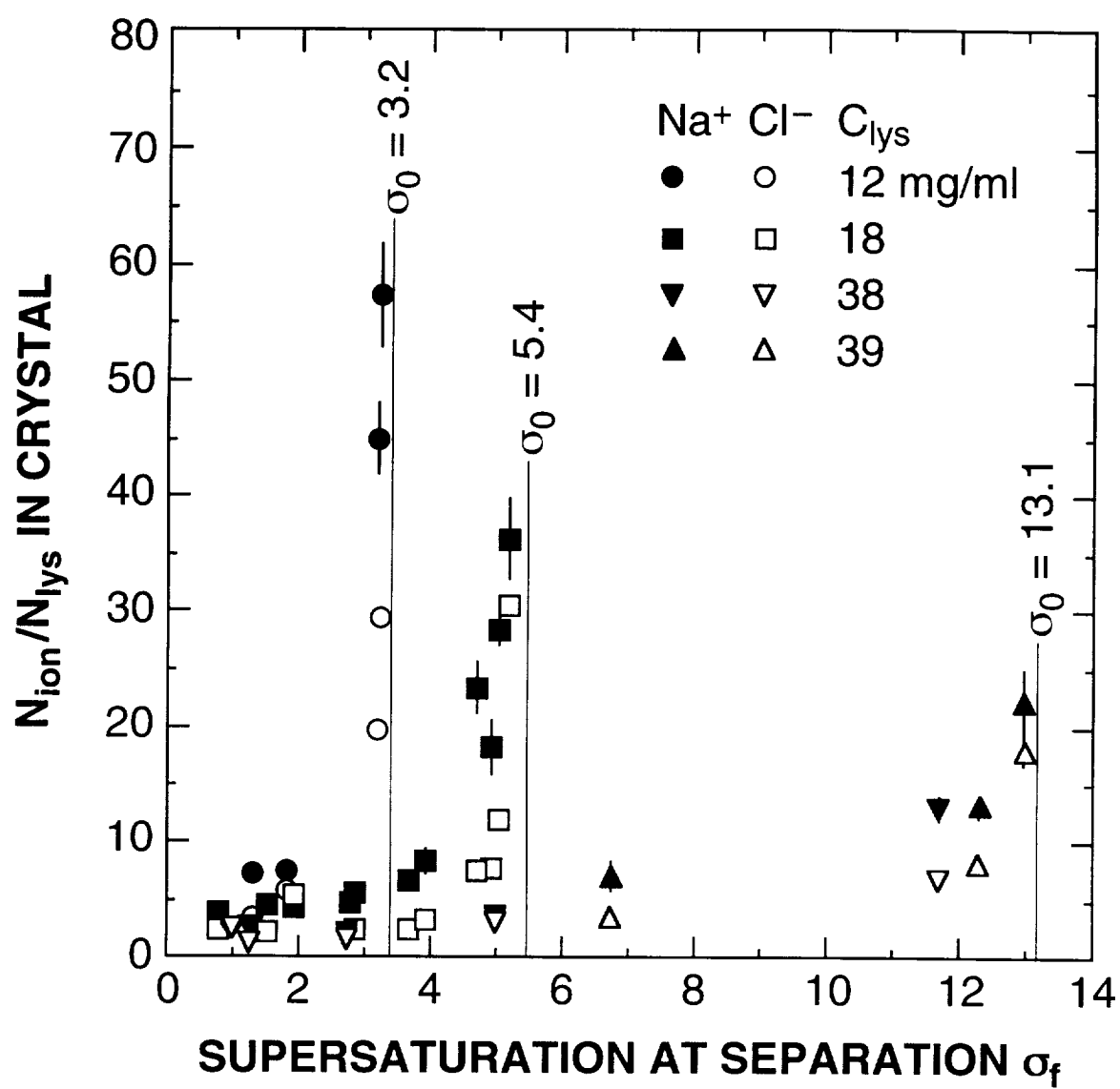
FIG. 6
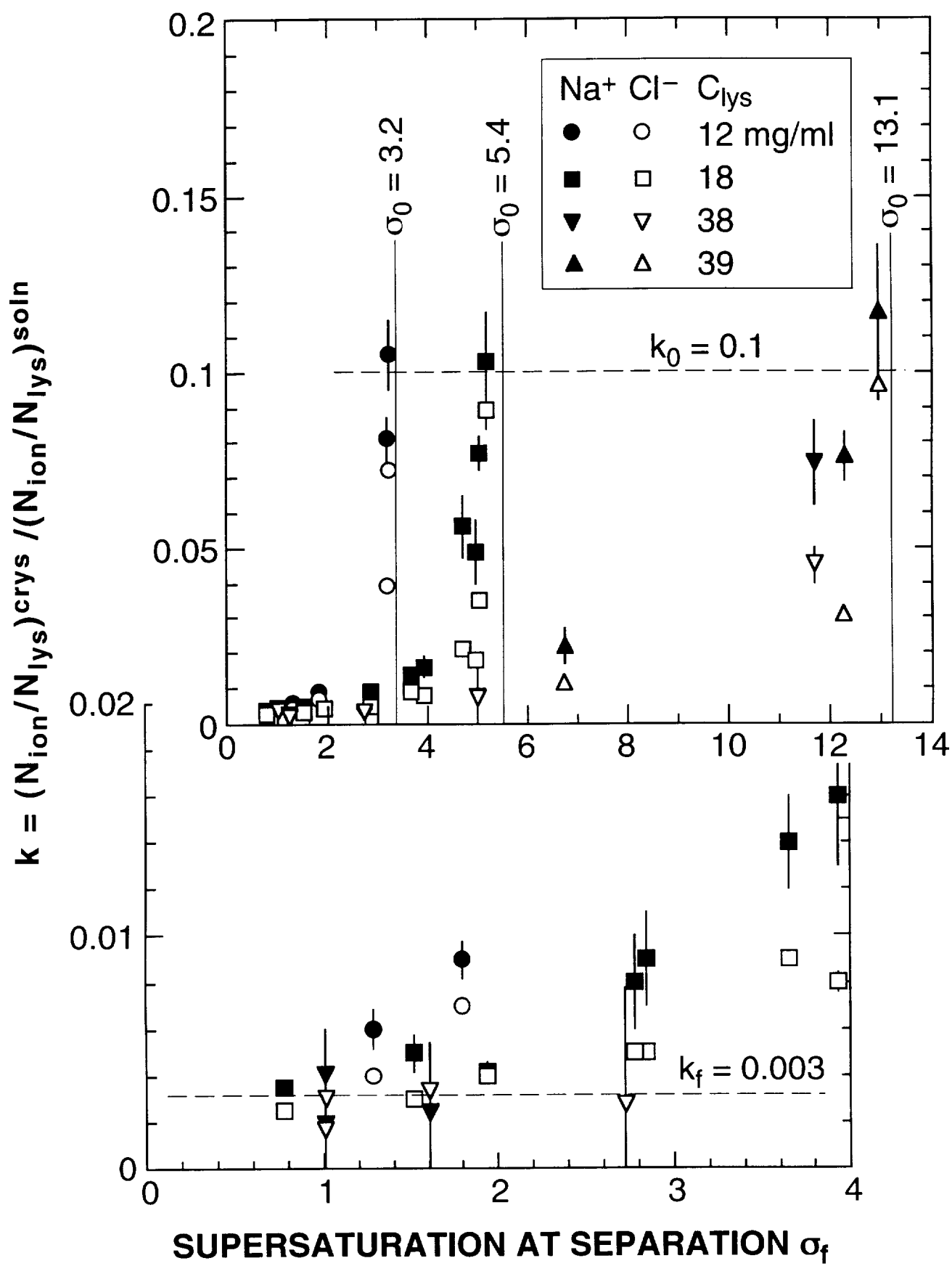
FIG. 7

FIG. 8
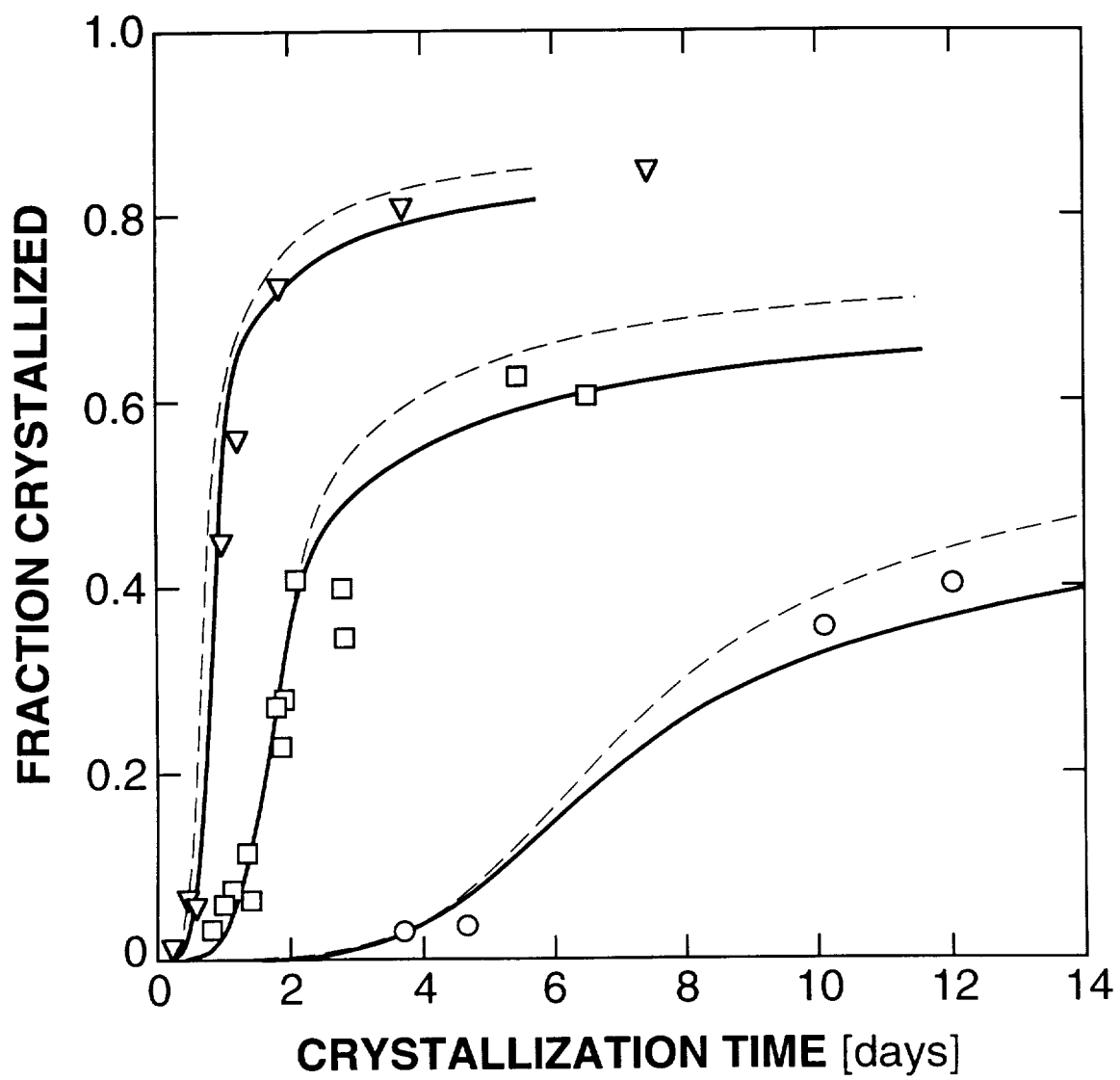
FIG. 9

FIG. 10

FIG. 11

LYSOZYME

50 mg/ml, pH 4.5
NaCl 2.5% w/v
T = 15˚C

θ = 15

Δt = 6 hr

RESCALED $G_2(\tau)$

DELAY TIME τ [μs]

FIG. 12

FIG. 13